Spiral diffusion of rotating self-propellers with stochastic perturbation

Amir Nourhani, Stephen J. Ebbens, John G. Gibbs, and Paul E. Lammert

Spiral diffusion of rotating self-propellers with stochastic perturbation

Amir Nourhani,[1,2,*] Stephen J. Ebbens,[3] John G. Gibbs,[4,5] and Paul E. Lammert[1,2,†]

[1]*Center for Nanoscale Science,The Pennsylvania State University, University Park, PA 16802, USA*
[2]*Department of Physics, The Pennsylvania State University, University Park, PA 16802, USA*
[3]*Department of Chemical & Biological Engineering, University of Sheffield, UK*
[4]*Department of Physics and Astronomy, Northern Arizona University, Flagstaff, Arizona 86011, USA*
[5]*Center for Bioengineering Innovation, Northern Arizona University, Flagstaff, Arizona 86011, USA*

Translationally diffusive behavior arising from the combination of orientational diffusion and powered motion at microscopic scales is a known phenomenon, but the peculiarities of the evolution of expected position conditioned on initial position and orientation have been neglected. A theory is given of the spiral motion of the mean trajectory depending upon propulsion speed, angular velocity, orientational diffusion and rate of random chirality reversal. We demonstrate the experimental accessibility of this effect using both tadpole-like and Janus sphere dimer rotating motors. Sensitivity of the mean trajectory to the kinematic parameters suggest that it may be a useful way to determine those parameters.

Active colloids such as microswimmers and nanomotors are a class of non-equilibrium systems which has been the subject of intense research in recent years [1–5]. At the sub-micron length scale, stochastic effects significantly perturb a self-propeller's deterministic motion, and the coupling of such noise to a steady motion can lead to unexpected emergent phenomena such as motility-induced phase separation [6], chiral diffusion [7], and phenomena with biological relevance [8] which can now be modelled by artificial active colloids. In the absence of noise a circle swimmer, confined to a plane with a strong rotational component to its powered motion, travels on a fixed circle with a steady clockwise or counterclockwise chirality [9]. Artificial swimmers of this sort have been fabricated in a variety of forms such as tadpoles [10, 11], Janus sphere dimers [12, 13], nanorods [14–16], and acoustically-activated swimmers [17]. Stochastic perturbations in the form of unbiased orientational diffusion or random chirality-reversal resulting from flipping about the direction of motion have significant effects on the long term motion: an effective translational diffusion is generated [18–20], the infinite-time limit of the mean position conditioned on the initial position and velocity is non-zero and chirality-dependent [7], and the mean approach to the limit is a logarithmic spiral [20, 21].

In this Letter, we experimentally and theoretically demonstrate "spiral diffusion" as a general finite-time behavior of the conditional mean position in circle swimmers. First, we expose the phenomenon in experimental data for both tadpole-like [11] and Janus-sphere dimer [12] rotary microswimmers (see Fig. 1), and present fits to the model. Then, we explain the theory for spiral diffusion of circle swimmers subjected to both orientational diffusion and flipping (change of chirality). The expected position of the swimmer, conditioned on its initial position, velocity direction and chirality, evolves

along a converging spiral. The theory serves as a sensitive and accurate utility for determining kinematic parameters such as angular velocity and orientational diffusivity. The appendix describes the details of fabrication and experimental protocols and the Supplementary Material contains movies of simulated ensembles of swimmers for a variety of deterministic and noise parameters.

Experiments were performed on two different rotor designs, tadpole-like microswimmers [11] and Janus sphere dimers [12]. The motors are denser than the aqueous solution of hydrogen peroxide, thus they move near the substrate and effectively confined to a horizontal plane. Even within a batch of nominally identical motors, there is usually a significant range of kinematic parameters. The analyzed experimental data consisted of two videos for each type of swimmer. From a single video of N
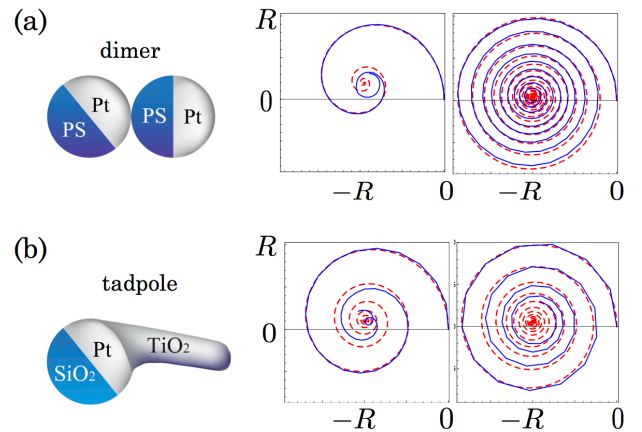

FIG. 1. (color online) Traces of mean trajectories (solid blue) of synthetic ensembles constructed from video of a single motor trajectory, along with fits to the theory (dashed red). Two trajectories for each of the motor types, (a) tadpoles and (b) Janus sphere dimers were selected for this investigation. The fit parameters (ω [rad/s], D_o [rad^2/s]) to trajectories for dimers are left: (0.86, 0.176) and right: (1.07, 0.037), and for tadpole-like swimmers are left: (4.26, 0.446) and right: (6.15, 0.321).
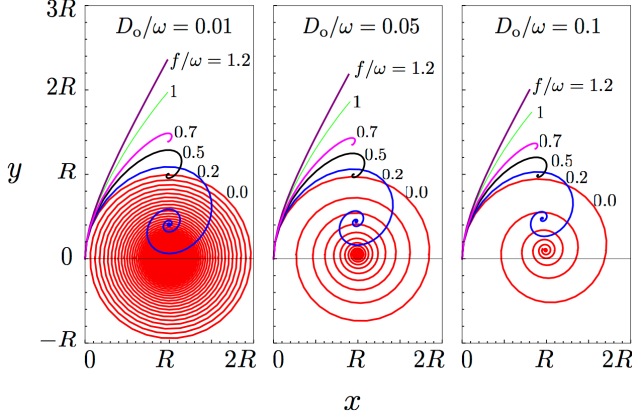
* nourhani@psu.edu
† lammert@psu.edu

FIG. 2. (color online) Traces of the mean position $\langle \boldsymbol{r}(t) \rangle$ of clockwise rotary self-propellers conditioned on initial position at the origin and initial velocity directed along $\hat{e}_y$, for dimensionless orientational diffusivity $D_{\mathrm{o}}/\omega = 0.01, 0.05$ and 0.1 and dimensionless flipping rate $f/\omega = 0, 0.2, 0.5, 0.7, 1$ and 1.2. According to Eqs. (3), (4), and (6), $\langle \boldsymbol{r}(t) \rangle$ spirals in to its asymptotic value when $f < \omega$, but the approach is non-oscillatory for $f > \omega$. Watch the videos in Supplementary Material [22] for a comparison of theory and simulation.

frames, an ensemble of N_{traj} trajectories, each of length $N - N_{\mathrm{traj}}$ frames is synthesized. For $1 \leq n \leq N_{\mathrm{traj}}$, the n-th member of the ensemble is obtained by taking frames n through $N - N_{\mathrm{traj}} + n - 1$ of the original video and rotating them so that the initial velocities are always in the same ($\hat{v}_0$) direction. Average positions of these synthesized ensembles are shown as solid blue spirals in Fig. 1. Fits to the theory, as explained below, are shown as dashed red curves, and are obtained by adjusting the angular speed ω, linear speed $v = R\omega$, and orientational diffusion coefficient D_{o}. With this method, we find a much more sensitive fit to these kinematic parameters than from working directly with the orientation time series and mean square displacement; a small change in the ratio D_{o}/ω can change the shape of the spiral.

To develop the theory, we begin with the deterministic part of a circle swimmer's motion. The particle moves with constant linear $\boldsymbol{v} = v\hat{v}$ and angular $\boldsymbol{\omega} = \omega\hat{\omega}$ ($\omega \geq 0$) velocities; The instantaneous orbit of motion has radius $R = v/\omega$ and the vector $\boldsymbol{p} = R\hat{p} = R\hat{v} \times \hat{\omega}$ connects the center of instantaneous orbit to the self-propeller. Assuming the particles start from the same initial position and velocity, the time-dependent right-handed body frame $\mathbf{E}(t) = [\hat{p}, \hat{v}, \hat{\omega}]^T(t)$ is related to the fixed laboratory frame by $\mathbf{E}(0) = [\hat{p}_0, \hat{v}_0, \hat{\omega}_0]^T = [\hat{x}, \hat{y}, \hat{z}]^T$ for counterclockwise rotation, ($\mathbf{E}(0) = [-\hat{x}, \hat{y}, -\hat{z}]^T$ for clockwise). To study the dynamics of these particles we use the kinematrix theory [23, 24], that we recently developed as an alternative to Langevin and Fokker-Planck formalisms. In the limit of short noise correlation and momentum relaxation times, the self-propeller's kinematic properties such as orientational diffusion, angular speed and flipping rate can be packaged into a 3×3 *kinematrix* $\mathcal{K}$. The dynamics of the body frame is governed by

$\frac{d}{dt}\langle \mathbf{E}(t) \rangle = -\mathcal{K}\langle \mathbf{E}(t) \rangle$ where $\langle \cdot \rangle$ is the ensemble average operator over all realization of noises. This model is appropriate to nanomotors and microswimmers at low Reynolds number, since the relaxation time due to viscous damping is very short (for a micron-sized object, of order 1 μs), and correlation times of environmental stochastic forces are even shorter.

The self-propeller moves near a plane in 2D ($\hat{v} \perp \hat{\omega}$), undergoing orientational diffusion with diffusivity D_{o} about $\hat{\omega}$ while, simultaneously and independently, it flips about its direction of motion $\hat{v}$ with frequency f and thereby reversing chirality. Although the motors in our experimental study had stable chirality, some artificial motors can experience flipping [14]. The kinematrix for this model is [23]

$$\mathcal{K} = \begin{bmatrix} D_{\mathrm{o}}{+}2f & \omega & 0 \\ -\omega & D_{\mathrm{o}} & 0 \\ 0 & 0 & 2f \end{bmatrix}. \qquad (1)$$

The stochastic motion of the body frame generates an effective (long-time) translational diffusivity

$$D_{\mathrm{eff}} = \frac{v^2}{2}\left[\mathcal{K}^{-1}\right]_{22} = \frac{\omega R^2}{2}\frac{\omega(D_{\mathrm{o}} + 2f)}{(D_{\mathrm{o}} + f)^2 + (\omega^2 - f^2)}. \qquad (2)$$

Passive translational diffusion with diffusivity D_t contributes an independent diffusion, so that the net diffusion coefficient is $D_{\mathrm{eff}} + D_t$. Passive translational diffusion is not coupled to the powered motion, but orientational diffusion is. It is for this reason that the latter can dominate the total diffusion. Random flipping instantaneously creates a large qualitative change in the motion and is alone sufficient to generate long-term diffusion.

The effective diffusivity D_{eff} tells us about the asymptotic behavior of the mean-squared displacement. At finite times, there are corrections which we will discuss later. But, more significant for the subject of this Letter is the mean displacement vector, given by

$$\langle \Delta \boldsymbol{r}(t) \rangle = v\left[\mathcal{K}^{-1}\left(\mathcal{I} - e^{-\mathcal{K}t}\right)\mathbf{E}(0)\right] \cdot \hat{v}_0$$
$$= \langle \Delta \boldsymbol{r} \rangle_\infty - 2\frac{D_{\mathrm{eff}}}{R}\boldsymbol{G}(t)e^{-(D_{\mathrm{o}}+f)t}, \qquad (3)$$

where the asymptotic value is

$$\langle \Delta \boldsymbol{r} \rangle_\infty = 2\frac{D_{\mathrm{eff}}}{R}\left(\frac{\hat{v}_0}{\omega} - \frac{\hat{p}_0}{D_{\mathrm{o}} + 2f}\right). \qquad (4)$$

The special case of this result for no flipping has been derived previously [21]. Translational diffusion does not affect $\langle \Delta \boldsymbol{r}(t) \rangle$. Instead, it reflects the interaction of *orientational* diffusion, chirality reversal, and powered rotation. The second term in the final expression of Eq. (3), which represents a transient, will be considered momentarily. To understand the expression (4) for the asymptotic mean displacement, it's helpful to unpack it a little in the low-noise limit. Expanding to first order in D_{o}
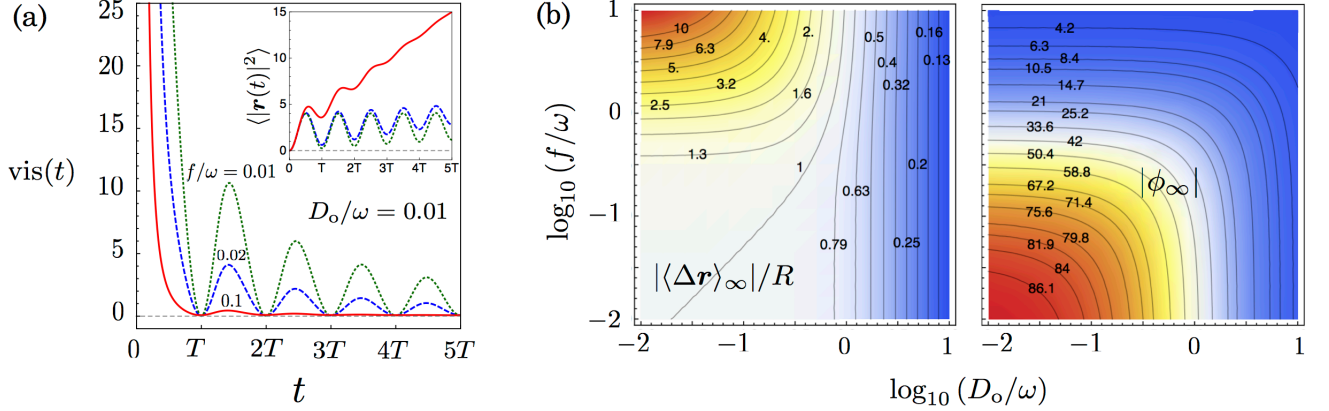
FIG. 3. (color online) (a) The visibility ratio vis$(t) = |\langle \boldsymbol{r}(t)\rangle|^2/\mathrm{var}(\boldsymbol{r}(t))$ measures the ease of discerning the mean behavior of $\boldsymbol{r}(t)$ against the background of its statistical spread. It drops to near zero more quickly the larger f and D_o. Inset: mean square displacement reaches the diffusive regime faster as $(f + D_\mathrm{o})/\omega$ increases. (b) Left: $|\langle \Delta \boldsymbol{r}\rangle_\infty|/R = 2(D_\mathrm{eff}/R^2)\sqrt{\omega^{-2} + (D_\mathrm{o} + 2f)^{-2}}$ as function of D_o/ω and f/ω. Right: $|\phi_\infty| = \tan^{-1}[\omega/(D_\mathrm{o} + 2f)]$, the magnitude of the angle between $\langle \Delta \boldsymbol{r}\rangle_\infty$ and $\hat{v}_0$, as function of D_o/ω and f/ω.

and f, we find

$$\frac{\langle \Delta \boldsymbol{r}\rangle_\infty}{R} \approx -\hat{p}_0 + \omega^{-1}(D_\mathrm{o} + 2f)\hat{v}_0. \tag{5}$$

In the limit of vanishing noise, $\langle \Delta \boldsymbol{r}\rangle_\infty$ tends to the time-average position for the deterministic motion on a circle. In the presence of noise, there is a deviation, but in the direction of the initial velocity.

Turning to the second (transient) term in Eq. (3), with the abbreviation $\alpha = \sqrt{\omega^2 - f^2}$, the vector $\boldsymbol{G}(t)$ is

$$\boldsymbol{G}(t) = \left[\cos\alpha t + \left(f - \frac{\omega^2}{D_\mathrm{o} + 2f}\right)\frac{\sin\alpha t}{\alpha}\right]\frac{\hat{v}_0}{\omega}$$
$$- \left[\cos\alpha t + (D_\mathrm{o} + f)\frac{\sin\alpha t}{\alpha}\right]\frac{\hat{p}_0}{D_\mathrm{o} + 2f}. \tag{6}$$

The asymptote $\langle \Delta \boldsymbol{r}\rangle_\infty$ has a more-or-less uniform qualitative behavior upon varying D_o and f. For the approach to the asymptote, on the other hand, there are two distinct regimes of f/ω (see Fig. 2). If $0 \le f < \omega$, $\boldsymbol{G}$ is purely oscillatory. Thus, the norm of $\langle \Delta \boldsymbol{r}(t)\rangle - \langle \Delta \boldsymbol{r}\rangle_\infty$ is bounded by a constant multiple of the decaying exponential $\exp[-(D_\mathrm{o} + f)t]$. Within that bound it oscillates, but the oscillation frequency α depends on f and goes to zero as f increases to ω. This is a little surprising; one might have expected that ω itself was the only possible oscillation frequency. If $\omega < f$, then $\boldsymbol{G}$ grows exponentially with rate $(f^2 - \omega^2)^{1/2}$. Thus, $|\langle \Delta \boldsymbol{r}(t)\rangle - \langle \Delta \boldsymbol{r}\rangle_\infty| \sim \exp\{-[D_\mathrm{o} + f - (f^2 - \omega^2)^{1/2}]t\}$ and the approach is non-oscillatory. At fixed D_o, the approach rate has a cusp at $f = \omega$, and tends to D_o for both $f = 0$ and $f \approx \infty$.

Figure 2 depicts traces of the clockwise rotors' mean trajectory conditioned on $\mathbf{E}(0) = [-\hat{x}, \hat{y}, -\hat{z}]^T$ for a range of values of D_o/ω and f/ω, according to the theory just developed. Although the temporal aspect is lost,

many of the features we have discussed can be seen there. If $D_\mathrm{o} = f = 0$, then the time average of $\Delta \boldsymbol{r}(t)$ is simply $-\hat{p}_0$. A small amount of noise should cause $\langle \Delta \boldsymbol{r}\rangle_\infty$ to deviate by only a small amount from that limit. More precisely, according to a formula derived earlier, $\langle \Delta \boldsymbol{r}\rangle_\infty$ should move up from the initial orbit center by $R(D_\mathrm{o} + 2f)/\omega$; Fig. 2 bears this out up to values of $f \approx \omega$. The number of visible oscillations decreases very rapidly with increasing noise. This is partly due to the increased damping and partly due to the decreased oscillation frequency [α in Eq. (6)]. For $f \gtrsim \omega$, oscillations no longer occur. Movies contained in Supplementary Information show simulated particle ensembles, along with their empirical mean positions; thereby, the temporal aspects can be better appreciated.

The orderly and revealing behavior of the mean displacement is very difficult to discern in a single trajectory without the sort of special processing we have used. This difficulty can be quantified, using the *visibility* of the mean displacement $\langle \Delta \boldsymbol{r}(t)\rangle$, defined as

$$\mathrm{vis}(t) = \frac{|\langle \boldsymbol{r}(t)\rangle|^2}{\mathrm{var}(\boldsymbol{r}(t))}, \tag{7}$$

where $\mathrm{var}(\boldsymbol{r}(t)) = \langle |\boldsymbol{r}(t)|^2\rangle - |\langle \boldsymbol{r}(t)\rangle|^2$ is the variance of the position at time t. If vis(t) is very small, we cannot expect to directly discern the mean behavior even in a small ensemble. The left panel of Fig. 3 shows plots of visibility at a range of f/ω values for $D_\mathrm{o} = 0.01\,\omega$. For $D_\mathrm{o} + f \sim 10^{-2}\omega$, the mean displacement is comparable to the spreading width, and vis(t) takes several periods to degrade. At larger values, $D_\mathrm{o} + f \gtrsim 10^{-1}\omega$, the effect is much weaker and visibility drops to near zero in less than one period.

Now we turn to a closer look at the long-time asymptote $\langle \Delta \boldsymbol{r}\rangle_\infty$ of the mean displacement. Although, as f increases, $\langle \Delta \boldsymbol{r}\rangle_\infty$ moves away from the ideal orbit center

in the direction of $\hat{v}_0$, it does not do so indefinitely; the $f \to \infty$ limit is $\omega R \hat{v}_0 / D_o$ $[= \boldsymbol{v}(0)/D_o]$. The center and right panels of Fig. 3 show details of the behavior of both the norm $|\langle \Delta \boldsymbol{r} \rangle_\infty| = 2(D_{\text{eff}}/R)\sqrt{\omega^{-2} + (D_o + 2f)^{-2}}$ and the absolute value $|\phi_\infty| = \tan^{-1}[\omega/(D_o+2f)]$ of the angle $\langle \Delta \boldsymbol{r} \rangle_\infty$ makes with $\hat{v}_0$ ("chiral angle"). As the flipping rate f or orientational diffusivity D_o increases, $|\phi_\infty|$ decreases. Since $\langle \Delta \boldsymbol{r} \rangle_\infty$ depends on f and D_o only through their ratio with ω, this limit can equivalently be thought of as $\omega \to 0$. From that perspective, the behavior is understandable as the circular (noise-free) trajectory degenerates to a straight line. However, in the experimentally relevant range, $D_o/\omega \sim 10^{-2} - 10^{-1}$, we always find a non-negligible chiral angle. In the limit of weak noise, $|\langle \Delta \boldsymbol{r} \rangle_\infty|$ is of the order of the radius of the deterministic trajectory. At high orientational diffusion, the particle changes its direction rapidly and therefore $|\langle \Delta \boldsymbol{r} \rangle_\infty|$ is smaller than the radius of the orbit. For $D_o \ll \omega$ and $f \gg \omega$ the motor effectively acts more like a rectilinear motor than a rotor, thus the magnitude of displacement is much larger than the radius of the orbit.

The asymptotic chiral angle is different. At low noise it is natural to preserve the chiral nature; the flipping rate is low and the deviation from circular trajectory is small. $|\phi_\infty|$ is very small both when $D_o \gg \omega$ and when $f \gg \omega$, but for different reasons. Large D_o implies that trajectories strongly deviate from the the chiral deterministic rotation; although chirality is preserved, its expression is very weak. With large f, on the other hand, the chirality itself is alternating rapidly. The asymptotic chiral angle reflects only the early memory of the initial chirality. After that, the rotor averages out to a linear motion.

In conclusion, we have shown that, in the presence of orientational diffusion and flipping, the expected position as a function of time of a rotary self-propeller, relative to its time-zero position and velocity, has significant structure related to the kinematic parameters. Using ensembles synthesized from single experimental trajectories, this structure is accessible and can be used to determine the kinematic parameters. The tell-tale spiral can be clearly seen over much shorter time scales than those required for the long-time effective diffusion to manifest itself.

Appendix A: Appendix: fabrication and experimental protocols

The "tadpole" microswimmer particles are fabricated the following way: a monolayer of $2\,\mu$m diameter silica microspheres (Bangs Laboratories, Inc., Fishers, IN) was deposited onto a clean silicon wafer [Si(100)] using a Langmuir-Blodgett technique. Subsequently, the substrate was placed into a physical vapor deposition system and thin films of $5\,$nm titanium adhesion layer followed by a $10\,$nm platinum catalyst were deposited onto the microbeads, forming half-coated Janus spheres. Then, the substrate was tilted by an in-vacuum motor to an oblique angle of $85°$ (the angle between the surface normal and the incident vapor direction). Later, a thick layer of titanium dioxide was deposited to a thickness of nearly $8\,\mu$m leading to rod-like formations on each microbead. The high-incidence angle deposition is known as Glancing Angle Deposition. After removing the substrate from the chamber, the tadpole structures were gently detached from the surface via bath sonication, suspending them into pure water of $18\,$MΩ resistance. The colloidal suspension was mixed with varying concentrations of hydrogen peroxide (fuel), and pipetted onto silicon wafers, previously cleaned by oxygen plasma (Harrick Plasma Ithaca, NY). The motion of the tadpoles was observed by brightfield microscopy using a Zeiss Axiophot microscope in reflection mode with a $40\times$ or $60\times$ dry objective coupled to a Mikrotron EoSens GE MC 1364 camera (Unterschleissheim, Germany). The particles' positions were tracked using the software ImageJ [25] and the plugin MTrack2 [26].

To fabricate the Janus sphere dimers, first, Janus catalytic beads were made by using a spin coater (Laurell Technologies Corp.) to deposit polystyrene colloids (0.1 % wt suspension in ethanol of 2 m diameter beads, Duke Scientific) onto a clean glass slide. Spin coating conditions were chosen to generate a separate non-touching distribution of colloids (typical conditions: 30 second spin, 2000 rpm, 100 L dispensed onto spinning substrate). These glass slides were then subject to directional platinum metal (Agar scientific, 99.9%) evaporation using a Moorfield Minilab 80 e-beam evaporator (5 nm coating thickness, monitored using a quartz-crystal oscillator). Damp lens tissue (Whatman) was then used to transfer the metallised colloids from the glass slide into a solution containing hydrogen peroxide (20 % w/v). The colloids were incubated for a few days in this solution, during which time agglomerates were observed to form, including the dimer swimmers that were studied in this paper. In order to explore spiral diffusion phenomena, the suspension of agglomerated swimmers prepared above was diluted to give a 10% w/v hydrogen peroxide concentration, and then placed into a low volume rectangular glass cuvette (Hellma). A Nikon Eclipse ME600 microscope operating in transmission mode was used to directly observe the movement of the colloids. Focus was arranged to ensure that only colloids remaining in close proximity

to one of the planar surfaces of the cuvette were investigated. A camera attached to the microscope (Pixelink PL-742) was used to record videos of the two body agglomerates motion (duration up to 1 hour, frame rate 3-15 Hz). These videos were subject to automated image analysis using a threshold algorithm to determine the centre of mass for each colloid in each frame with sub-pixel accuracy, output as time-stamped trajectories (custom software developed using the National Instruments Labview platform).

[1] K. Kim, J. Guo, Z. X. Liang, F. Q. Zhuc, and D. L. Fan, Nanoscale **8**, 10471 (2016).

[2] C. Bechinger, R. D. Leonardo, H. Löwen, C. Reichhardt, G. Volpe, and G. Volpe, Rev. Mod. Phys., arXiv:1602.00081 (2016).

[3] C. O. Reichhardt and C. Reichhardt, arXiv:1604.01072 (2016).

[4] P. E. Lammert, V. H. Crespi, and A. Nourhani, J. Fluid Mech. **802**, 294 (2016).

[5] A. Nourhani, V. H. Crespi, and P. E. Lammert, Phys. Rev. E **91**, 062303 (2015).

[6] J. Tailleur and M. E. Cates, Phys. Rev. Lett. **100** (2008).

[7] A. Nourhani, P. E. Lammert, A. Borhan, and V. H. Crespi, Phys. Rev. E **87** (2013).

[8] B. M. Friedrich and F. Jülicher, New Journal of Physics **10**, 123025 (2008).

[9] A. Nourhani, Y.-M. Byun, P. E. Lammert, A. Borhan, and V. H. Crespi, Phys. Rev. E **88**, 062317 (2013).

[10] J. G. Gibbs and Y. Zhao, Small **6**, 1656 (2010).

[11] J. G. Gibbs, S. Kothari, D. Saintillan, and Y. P. Zhao, Nano Letters **11**, 2543 (2011).

[12] S. Ebbens, R. A. L. Jones, A. J. Ryan, R. Golestanian, and J. R. Howse, Phys. Rev. E **82** (2010).

[13] L. F. Valadares, Y.-G. Tao, N. S. Zacharia, V. Kitaev, F. Galembeck, R. Kapral, and G. A. Ozin, Small **6**, 565 (2010).

[14] D. Takagi, A. B. Braunschweig, J. Zhang, and M. J. Shelley, Phys Rev. Lett. **110**, 038301 (2013).

[15] Y. Wang, S. to Fei, Y.-M. Byun, P. E. Lammert, V. H. Crespi, A. Sen, and T. E. Mallouk, J Am Chem Soc **131**, 9926 (2009).

[16] A. Nourhani and P. E. Lammert, Phys Rev. Lett. **116**, 178302 (2016).

[17] D. Ahmed, M. Lu, A. Nourhani, P. E. Lammert, Z. Stratton, H. S. Muddana, V. H. Crespi, and T. J. Huang, Scientific Reports **5**, 9744 (2015).

[18] D. Debnath, P. K. Ghosh, Y. Li, F. Marchesoni, and B. Lid, Soft Matter **12**, 2017 (2016).

[19] P. Jung, G. Marchegiani, and F. Marchesoni, Phys. Rev. E **93**, 012606 (2016).

[20] F. Kummel, B. ten Hagen, R. Wittkowski, I. Buttinoni, R. Eichhorn, G. Volpe, H. Lowen, and C. Bechinger, Phys Rev. Lett. **110**, 198302 (2013).

[21] S. Teeffelen and H. Löwen, Phys. Rev. E **78**, 020101 (2008).

[22] See Supplemental Material at [URL will be inserted by publisher] for videos.

[23] A. Nourhani, P. E. Lammert, A. Borhan, and V. H. Crespi, Phys. Rev. E **89**, 062304 (2014).

[24] A. Nourhani, V. H. Crespi, and P. E. Lammert, Phys. Rev. E **90**, 062304 (2014).

[25] C. A. Schneider, W. S. Rasband, and K. W. Eliceiri, Nature Methods **9**, 671 (2012).

[26] D. R. Klopfenstein and R. D. Vale, Mol Biol Cell **15** (2004).